JACS
JOURNAL OF THE AMERICAN CHEMICAL SOCIETY
Article
pubs.acs.org/JACS

Multicomponent Nanomaterials with Complex Networked Architectures from Orthogonal Degradation and Binary Metal Backfilling in ABC Triblock Terpolymers

Christina D. Cowman,[†,⊥] Elliot Padgett,[‡] Kwan Wee Tan,[§] Robert Hovden,[‡] Yibei Gu,[§] Nina Andrejevic,[‡] David Muller,[‡] Geoffrey W. Coates,*[,†] and Ulrich Wiesner*[,§]

[†]Department of Chemistry and Chemical Biology, Cornell University, Baker Laboratory, Ithaca, New York 14853, United States
[‡]Department of Applied and Engineering Physics, Cornell University, Clark Hall, Ithaca, New York 14853, United States
[§]Department of Materials Science and Engineering, Cornell University, Bard Hall, Ithaca, New York 14853, United States

Supporting Information

ABSTRACT: Selective degradation of block copolymer templates and backfilling the open mesopores is an effective strategy for the synthesis of nanostructured hybrid and inorganic materials. Incorporation of more than one type of inorganic material in orthogonal ways enables the synthesis of multicomponent nanomaterials with complex yet well-controlled architectures; however, developments in this field have been limited by the availability of appropriate orthogonally degradable block copolymers for use as templates. We report the synthesis and self-assembly into cocontinuous network structures of polyisoprene-*block*-polystyrene-*block*-poly(propylene carbonate) where the polyisoprene and poly(propylene carbonate) blocks can be orthogonally removed from the polymer film. Through sequential block etching and backfilling the resulting mesopores with different metals, we demonstrate first steps toward the preparation of three-component polymer−inorganic hybrid materials with two distinct metal networks. Multiblock copolymers in which two blocks can be degraded and backfilled independently of each other, without interference from the other, may be used in a wide range of applications requiring periodically ordered complex multicomponent nanoarchitectures.

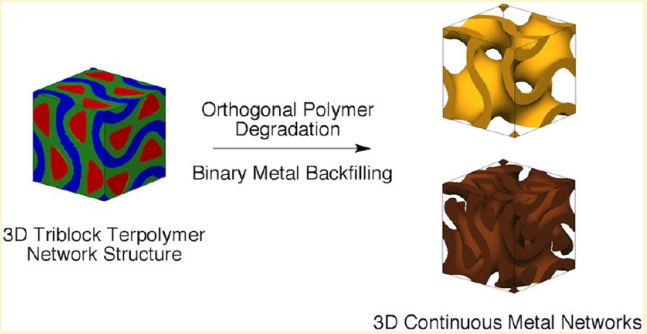

INTRODUCTION

Block copolymers self-assemble on the 10−100 nm length scale and are attractive materials to structure direct inorganic components into materials with mesoscale features.[1,2] Examples include nanostructured oxides, carbons, metals and semiconductors.[3−8] One route to such materials involves the use of block copolymers as sacrificial templates.[9] This strategy involves selective degradation of one polymer block to form ordered mesoporous structures and deposition of inorganic materials into the open mesopores. In particular, this approach has been used for the synthesis of inorganic network structures for metals and metal oxides.[10−15]

The incorporation of two distinct inorganic components into the same block copolymer template enables the fabrication of previously unknown classes of complex, multifunctional materials for a wide range of potential applications. First efforts toward this goal have been described. Thomas and co-workers reported coassembly of a binary mixture of SiO_2 and Au nanocrystals of different sizes with a lamellar-forming diblock copolymer. The segregation of the nanocrystals to different areas within the structure was based primarily on entropic contributions.[16] Alternatively, Li et al. demonstrated synthesis of ordered metal networks from coassembly of ABC triblock terpolymers and a mixture of Pt and Au nanoparticles, where the Pt and Au nanoparticles localized in specific areas within the structure based on ligand chemistry.[17] Stamm and co-workers reported orthogonal deposition of two different metal nanoparticles into different domains of block copolymer thin films. This process was achieved through a combination of coassembly with the first polymer domain and nanoparticle deposition using adsorption to the second polymer domain in a separate processing step. Stepwise nanoparticle dispersion so far is limited to thin film templates.[18] Furthermore, in no previous examples have two inorganic components been orthogonally deposited into two different domains of bulk block copolymer films via an etching and backfilling mechanism. Using a templating approach would require block copolymers that can be orthogonally degraded and backfilled. With orthogonality here we mean that two of the three blocks of the ABC terpolymer can be degraded and backfilled independently from one another, without interference from the other.

Received: February 20, 2015
Published: April 2, 2015

DOI: 10.1021/jacs.5b01915
J. Am. Chem. Soc. 2015, 137, 6026−6033

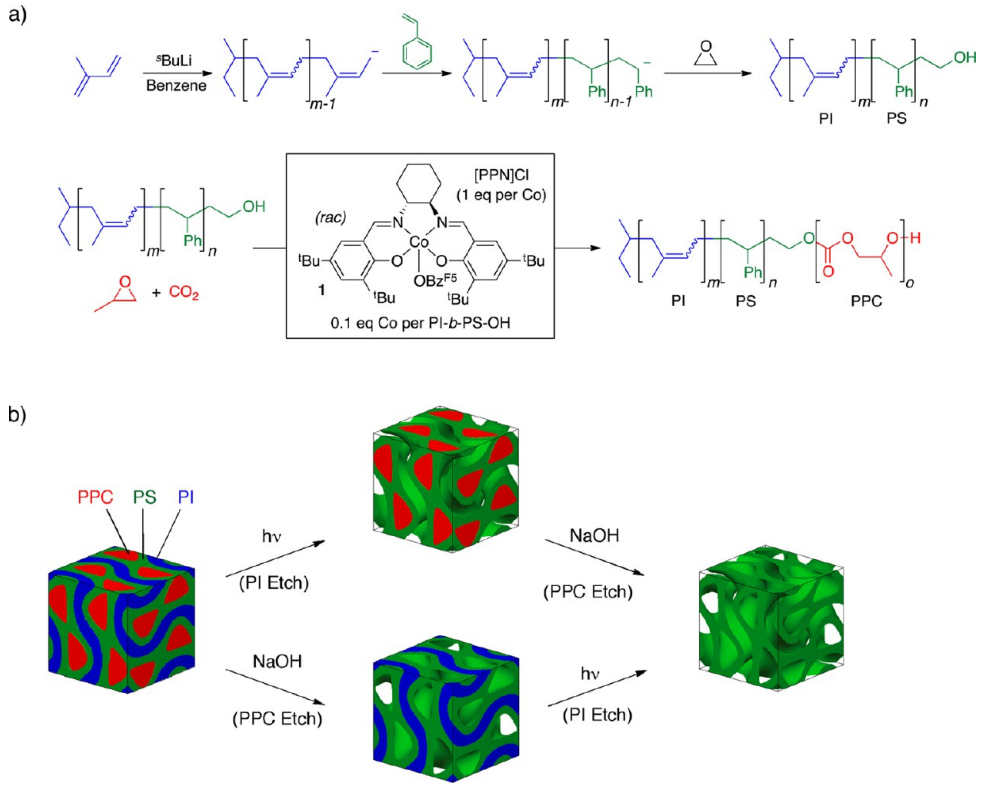

Figure 1. Synthesis and orthogonal degradation schemes of ABC triblock terpolymer PI-*b*-PS-*b*-PPC. (a) Synthesis of PI-*b*-PS-OH using anionic polymerization and synthesis of PI-*b*-PS-*b*-PPC triblock terpolymers from the parent PI-*b*-PS-OH diblock copolymer using rapid chain-shuttling polymerization of propylene oxide and CO_2 using **1**. (b) Schematic illustrating orthogonal degradation of PI and PPC blocks of PI-*b*-PS-*b*-PPC from a Q^{230} core–shell double gyroid structure using 302 nm UV light and NaOH.

ABC triblock terpolymers where two different blocks could be removed orthogonally would enable fabrication of composites constituted by two distinct inorganic materials in two different domains separated by a third polymer domain. In the case of triply periodic network structures, two separate networks could be sequentially degraded and the resulting porous structures backfilled, providing access to triply periodic composite structures. ABC triblock terpolymers and their composites benefit from the formation of triply periodic network morphologies over larger composition regions than diblock copolymers.[19,20] In addition, their use opens potential pathways to remove the remaining third block after orthogonal backfilling to produce porosity in the final composite structure.

To that end, we synthesized a series of new triblock terpolymers of polyisoprene-*block*-polystyrene-*block*-poly(propylene carbonate) (PI-*b*-PS-*b*-PPC) that self-assemble into cocontinuous network morphologies including the Q^{214} alternating gyroid, O^{70} orthorhombic network, and Q^{230} core–shell double gyroid morphologies and have orthogonal degradability of the polyisoprene (PI) and poly(propylene carbonate) (PPC) end blocks in bulk films. The PI block was degraded using irradiation with UV light, and the PPC block was labile in basic solutions. Via electroless plating and seeded growth deposition Au, Ni, and Cu metals were deposited into the mesoporous channels produced by degradation of either the PI or PPC blocks, as evidenced by transmission electron microscopy (TEM). As a proof of principle, we report the orthogonal deposition of Au and Cu metal into a single polymer template through sequential degradation and backfilling of the PI and PPC blocks, respectively. Incorporation of Au and Cu metal was characterized using high-angle annular dark field scanning transmission electron microscopy (HAADF STEM) and HAADF STEM tomography. The polystyrene (PS) block could be removed from the final composite structures by pyrolysis or dissolution to remove any remaining organic material.

EXPERIMENTAL SECTION

Salen Co(III) complex (**1**) was prepared according to previous literature procedures.[21] PI-*b*-PS-OH (Supporting Information), **1**, and [PPN]Cl were added to a 150 mL Fischer–Porter bottle in a glovebox. Propylene oxide was added to the reactor to produce the following concentrations: [PI-*b*-PS-OH] = 14 mM, [**1**] = 1.4 mM, [PPN]Cl = 1.4 mM. The reactor was sealed in the glovebox, removed and pressurized to 6.8 atm with CO_2. The polymerization was stirred at 21 °C. The length of the poly(propylene carbonate) (PPC) block produced is proportional to the reaction time. After the desired chain length is achieved, the reactor was depressurized, and the polymerization was quenched by adding methanol. A small amount of PPC homopolymer is produced during the rapid chain-shuttling polymerization of PPC due to initiation from the pentafluorobenzoate and chloride anions on the catalyst and cocatalyst, respectively.[21] The PI-*b*-PS-*b*-PPC triblock terpolymer was purified by dissolving precipitated polymer in minimal amounts of THF, and adding methanol to precipitate the polymer from solution. The dissolution and precipitation process was repeated a total of three times to remove residual **1**, [PPN]Cl salt, and PPC homopolymer from the PI-*b*-PS-*b*-PPC. Solvents were removed under reduced pressure.

Polymer overlayers were removed from the film surfaces using air plasma in a Harrick plasma cleaner. Films were plasma cleaned for 10 min and removed from the plasma cleaner and turned over a total of four times for a total of 40 min of plasma treatment.

UV degradation was performed using a UVP EL-series 8W lamp with a wavelength of 302 nm. Plasma-cleaned polymer films were

DOI: 10.1021/jacs.5b01915
J. Am. Chem. Soc. 2015, 137, 6026–6033

Table 1. PI-*b*-PS-*b*-PPC Triblock Terpolymers Identified in This Study with Co-continuous Network Morphologies and Their Characterization

entry	composition[a]	composition (vol %) (PI:PS:PPC)	M_n[b] (kg/mol)	M_w/M_n[b]	structure[c]	unit cell size (nm)[d]
1	PI_{128}-*b*-PS_{150}-*b*-PPC_{70}	31.9:49.3:18.8	35.5	1.10	O^{70}	82.1
2	PI_{130}-*b*-PS_{154}-*b*-PPC_{43}	34.3:53.5:12.2	31.6	1.12	Q^{214}	37.4
3	PI_{130}-*b*-PS_{154}-*b*-PPC_{75}	31.4:49.0:19.6	33.6	1.12	Q^{230}	71.3
4	PI_{156}-*b*-PS_{204}-*b*-PPC_{87}	30.1:51.8:18.1	39.6	1.11	Q^{230}	73.1

[a]Determined by ^{1}H NMR spectroscopy in $CDCl_3$ (400 MHz; n = 8, d_1 = 10s, PW = 45). Subscripts denote number of monomers in each block [b]Determined by GPC in THF at 30 °C vs PS standards. [c]Determined by a combination of SAXS and TEM. [d]The structure of terpolymer 1 was assigned to a O^{70} network structure with orthorhombic lattice and lattice parameters of a = 33.9 nm, b = 49.4 nm, and c = 82.1 nm (vide infra).

irradiated with 302 nm UV light to selectively degrade the PI block. The polymer films were placed at a distance of 3 in. under an 8W 302 nm UV lamp for 72 h. The polymer films were soaked in methanol for 48 h to remove any small molecule degradation products. The UV treatment cross-links the PS block slightly, which appears as a broadening of the molar mass distribution of the polymers from dissolved films by GPC after UV treatment. Cross-linking of the PS to the point of insolubility was observed only for the top surface of the polymer film; the amount of insoluble material was too small to be quantified by mass. No adverse effects on the PPC block after UV treatment were observed.

Plasma-cleaned polymer films were soaked in a solution of 1.25 M NaOH:methanol at a 1:2 ratio by volume for 60 h to selectively degrade the PPC block. Small-molecule degradation products were removed by soaking the degraded films in methanol for 48 h. No adverse effects on the PS or PI blocks were observed after degradation with NaOH.

The two degradation processes (UV and NaOH) are orthogonal. Rather than the degradation sequence PI first and then PPC, the degradation order can be reversed, degrading the PPC block first and then the PI block (i.e., NaOH first, followed by UV degradation).

Electroless and seeded growth deposition procedures can be found in the Supporting Information.

RESULTS AND DISCUSSION

PI-*b*-PS-*b*-PPC Triblock Terpolymer Synthesis. We synthesized a series of new orthogonally degradable PI-*b*-PS-*b*-PPC triblock terpolymers using a combination of anionic and rapid chain-shuttling polymerization (Figure 1a).[22,23] In rapid chain-shuttling polymerization (also called immortal polymerization), the polymerization reaction is catalyzed using a Lewis acid catalyst in the presence of chain-shuttling agents (CSAs) such as alcohols. When the rate of chain-shuttling between CSAs is faster than the rate of monomer incorporation, controlled molar masses and narrow molar mass distributions result.[22,23] Rapid chain-shuttling polymerization is the catalytic variant of a living polymerization, requiring substoichiometric amounts of catalyst relative to the number of chains produced in the polymerization, rather than stoichiometric amounts of an initiator. Polyisoprene-*b*-polystyrene diblock copolymers were synthesized using the sequential living anionic polymerization of isoprene and styrene and terminated with a hydroxyl group (PI-*b*-PS-OH) to act as macro-chain-shuttling agents.[24] Poly(propylene carbonate) was grown off of the macro-chain-shuttling agents via the alternating copolymerization of propylene oxide and CO_2 by a salen Co(III) complex (**1**) and a bis(triphenylphosphine)iminium chloride ([PPN]Cl) cocatalyst.[21,25−27] We chose a polycarbonate block to potentially tune the block chemistry through functionalized terminal epoxides and for potential resistance of the polycarbonate block to oxidative conditions. We designed the new PI-*b*-PS-*b*-PPC triblock terpolymer to have orthogonal degradability and found the PI and PPC blocks could be removed via irradiation with 302 nm UV light and NaOH, respectively (Figure 1b).

Self-Assembly of PI-*b*-PS-*b*-PPC. We mapped out sections of the PI-*b*-PS-*b*-PPC phase space to locate compositions where the triblock terpolymers self-assembled into cocontinuous network structures such as the cubic Q^{214} alternating gyroid, the orthorhombic O^{70} network, and the cubic Q^{230} core−shell double gyroid morphologies.[28,29] In the Q^{214} alternating gyroid, the structure is made up of two chemically distinct minority gyroid networks of PI and PPC, respectively, embedded in a matrix of the PS block.[29] Similarly, in the O^{70} network structure, the structure consists of two chemically distinct orthorhombic continuous minority networks of PI and PPC, respectively, embedded in a matrix of PS.[28,30,31] Finally, in the Q^{230} core−shell double gyroid the structure is made up of two gyroid minority networks of PPC coated with a shell of PS. In this case, the PI domain constitutes the matrix.[29] Different PI-*b*-PS-*b*-PPC triblock terpolymers and their compositions for which we identified these self-assembled network structures are summarized in Table 1. PI-*b*-PS-*b*-PPC terpolymers from Table 1 will be referred to as PI-*b*-PS-*b*-PPC-X, where X denotes Table 1 entry number.

Film structures formed during self-assembly of PI-*b*-PS-*b*-PPC triblock terpolymers were characterized using a combination of small-angle X-ray scattering (SAXS) as well as transmission and scanning electron microscopy (TEM and SEM). SAXS patterns for the polymers from Table 1 and analysis can be found in the Supporting Information (Figure S6−S8).

Orthogonal Degradation of PI-*b*-PS-*b*-PPC. Selective polymer degradation of one block has been reported for block copolymers containing polyesters, poly(methyl methacrylate), polyisoprene, polybutadiene, poly(ethylene oxide) and polysiloxanes.[9,11,13,32−37] Hillmyer and co-workers reported the synthesis of mesoporous polylactide through selective degradation of polybutadiene with internal olefin metathesis.[38] Emrick and co-workers reported orthogonal degradation of disulfide and phosphoester-functionalized polyolefin triblock terpolymers dissolved in solution but did not backfill nor characterize resulting porous solids.[39] Hillmyer and co-workers reported orthogonal degradation of ABC triblock terpolymer thin films of polyisoprene-*block*-polystyrene-*block*-polylactide, where the polyisoprene block was degraded using ozonolysis, and the polylactide block was degraded using sodium hydroxide.[40] However, ozonolysis of the triblock partially degraded the polylactide block in addition to the polyisoprene block, and removal in bulk polymer films was not demonstrated. Additionally, Hawker and co-workers reported the orthogonal degradation of thin films of a supramolecular complex of poly(ethylene oxide)-trityl-*b*-poly(styrene-*r*-4-hydroxystyrene) and poly(styrene-*r*-4-vinylpyridine)-*b*-poly-

DOI: 10.1021/jacs.5b01915
J. Am. Chem. Soc. 2015, 137, 6026−6033

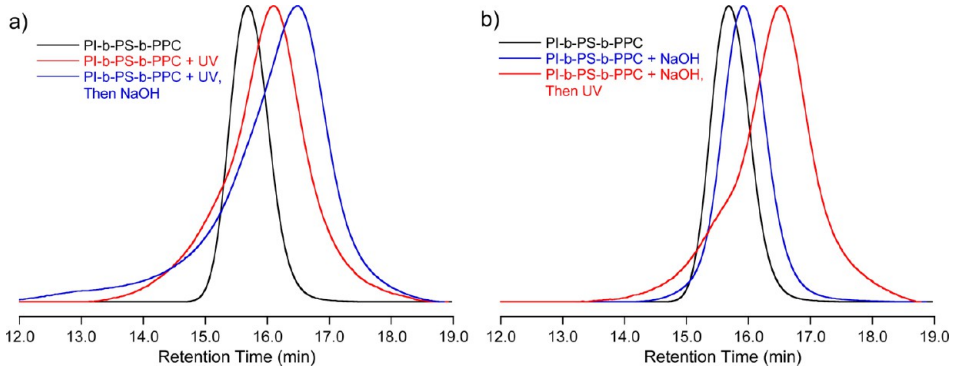

Figure 2. Orthogonal degradation of PI-*b*-PS-*b*-PPC polymer films (Q^{230} and O^{70}) as evidenced by GPC. (a,b) GPC traces of PI-*b*-PS-*b*-PPC-1 polymer films after (a) degradation of the PI (matrix) blocks followed by degradation of the PPC (gyroid minority networks) blocks; (b) degradation of the PPC blocks followed by degradation of the PI blocks.

(methyl methacrylate).[41] Orthogonal degradation was demonstrated by acid cleavage of the trityl ether linkage and UV degradation of the poly(methyl methacrylate) blocks. Again, orthogonal degradation was not demonstrated in bulk films.

In contrast, the PI and PPC blocks of PI-*b*-PS-*b*-PPC triblock terpolymers were orthogonally degradable in bulk films. The PI block was degraded using 302 nm UV light, and the PPC block was degraded by soaking the polymer film in a solution of NaOH. Irradiation of the block copolymers with 302 nm UV light in the presence of oxygen resulted in degradation of the PI blocks and cross-linking of the PS blocks with no apparent effects on the PPC blocks as evidenced by gel-permeation chromatography (GPC, Figure 2) and ^{1}H NMR spectroscopy (Supporting Figures S9–S12). The NaOH solution did not affect the PS or PI blocks. After each subsequent degradation step, in GPC we observed a clear shift of the polymer to lower molar mass (Figure 2a,b).

Orthogonal degradability was demonstrated on PI-*b*-PS-*b*-PPC-1 (O^{70} network structure) and PI-*b*-PS-*b*-PPC-3 (Q^{230} core–shell double gyroid) using gel permeation chromatography (GPC, Figure 2) and scanning electron microscopy (SEM, Figure 3). In the experiment leading to GPC traces in Figure 2a, the PI block was degraded first, resulting in a shift in the GPC trace to lower molar mass and broadening of the molar mass distribution, especially on the high molar mass side. This broadening is due to weak cross-linking of the PS block still allowing GPC analysis. Polymer films retained their network structure after removal of the PI blocks as evidenced by SEM (Figure 3a). Next, the PPC block was degraded using NaOH solution; as a result, we observed a further shift in the broadened GPC trace to lower molar mass. After removal of the PI and PPC blocks (~51 vol %), the periodic network structures were retained as suggested by the SEM micrograph in Figure 3c. Alternatively, in experiments leading to the traces in Figure 2b, the PPC block was degraded first, resulting in a shift to lower molar mass and retention of the narrow molar mass distribution. Structures were retained after PPC block removal as evidenced by SEM (Figure 3b). Next, the PI block was degraded using UV light resulting in a further shift of the GPC trace to lower molar mass as well as broadening of the molar mass distribution due to weak PS cross-linking (vide supra). The PS domains also retained their original structure after removal of the two end blocks in sequence: PPC first and then PI, as suggested by the SEM micrograph in Figure 3d. From the SEM and GPC data sets, we demonstrated that degradation of the PI and PPC blocks can be performed orthogonally with retention of the original block copolymer structure.

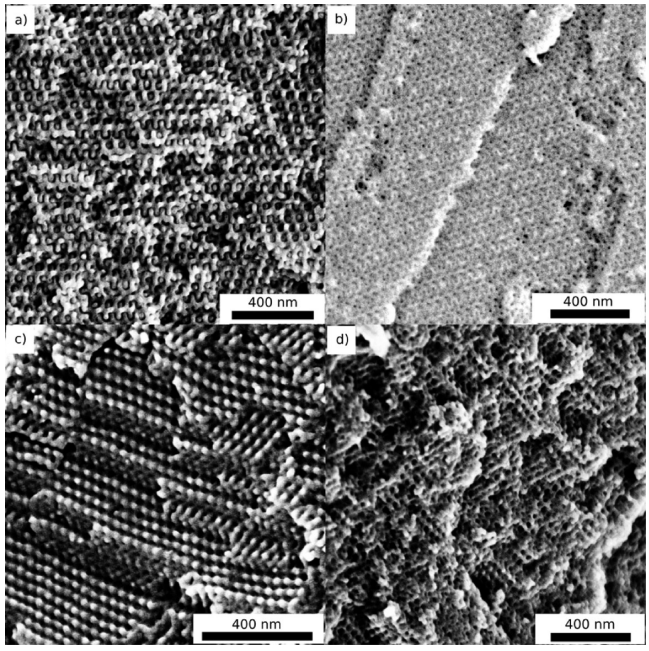

Figure 3. Orthogonal degradation of PI-*b*-PS-*b*-PPC polymer films (Q^{230} and O^{70}) as evidenced by SEM micrographs of the corresponding polymer film cross sections after (a) degradation of PI blocks only (PI-*b*-PS-*b*-PPC-3); (b) degradation of PPC blocks only (PI-*b*-PS-*b*-PPC-3); (c) degradation of PI blocks followed by degradation of PPC blocks (PI-*b*-PS-*b*-PPC-1); (d) degradation of PPC blocks followed by degradation of the PI blocks (PI-*b*-PS-*b*-PPC-1).

The SEM micrographs in Figure 3 are high-magnification images showing local structure retention after different sequences of PI and PPC block removal. A low-magnification SEM micrograph showing mesoporosity over the entire field of view for a film cross-section can be found in the Supporting Information (Figure S13a). Furthermore, SEM micrographs of film surfaces after removal of the PI and PPC blocks (Figure S13b and S13c, respectively) demonstrate that the film surfaces were porous after degradation, allowing for diffusion of metal plating solutions into the mesoporous polymer templates (vide infra).

Backfilling of PI-*b*-PS-*b*-PPC Templates with Metals. We used electroless and seeded growth deposition to backfill

DOI: 10.1021/jacs.5b01915
J. Am. Chem. Soc. 2015, 137, 6026–6033

Au, Cu, and Ni metal into mesoporous templates produced by orthogonally degrading the PI and PPC blocks of the networked PI-*b*-PS-*b*-PPC templates. Electroless and seeded growth deposition were used, as they do not require conducting substrates and have been demonstrated to be effective for block copolymer template systems.[10,11,42−44] Mesopores from both PI and PPC degradation were presumed to be hydrophilic from a mixture of carboxylic acids and hydroxyl groups formed by PI degradation[45,46] and from PPC degradation, respectively. Electroless deposition of Ni metal into gyroidal mesoporous templates has been reported by Hashimoto and co-workers,[11] Hsueh et al.,[42] and du Sart et al.[43] Au metal was backfilled using a seeded growth process adapted from work reported by Ho and co-workers.[47] Sita and co-workers demonstrated Cu metal deposition into lamellar block copolymer templates using electroless deposition.[48] TEM micrographs of resulting structures after deposition of Au, Ni, and Cu metal separately into the PI and PPC pores from various PI-*b*-PS-*b*-PPC terpolymer templates are shown in Figure 4. Au, Ni, and Cu

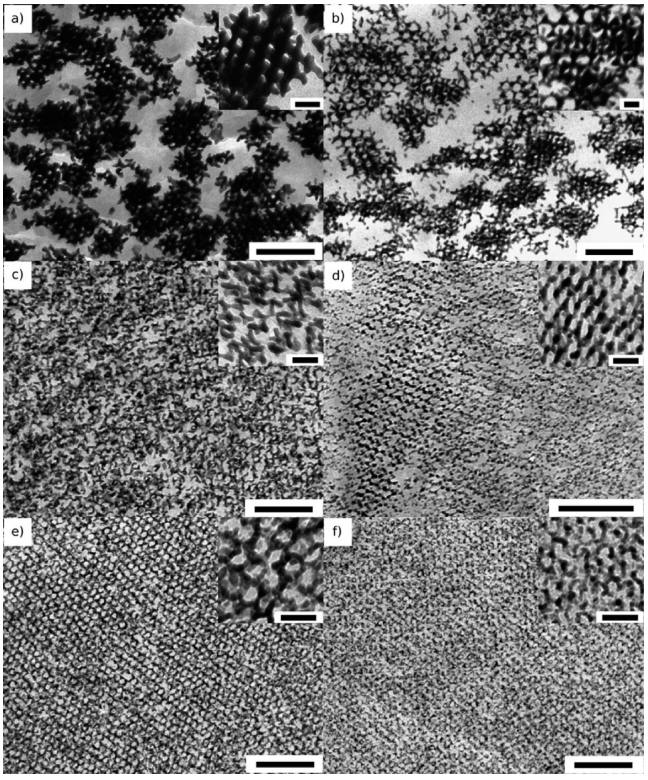

Figure 4. TEM micrographs of metal deposited into networked porous templates using electroless deposition (Cu, Ni), and seeded growth deposition (Au). Scale bars indicate 250 nm; inset scale bars indicate 50 nm. (a) Deposition of Au in PI pores (PI-*b*-PS-*b*-PPC-4) and (b) PPC pores (PI-*b*-PS-*b*-PPC-3). (c) Deposition of Ni metal into PI pores (PI-*b*-PS-*b*-PPC-4) and (d) PPC pores (PI-*b*-PS-*b*-PPC-1). (e) Deposition of Cu metal into matrix PI pores (PI-*b*-PS-*b*-PPC-4) and (f) minority network in PI pores (PI-*b*-PS-*b*-PPC-2).

metal appear dark in the TEM micrographs, providing contrast in the images. We backfilled the PI matrix pores of PI-*b*-PS-*b*-PPC-4 (Q^{230} core−shell double gyroid) with Au (Figure 4a), Ni (Figure 4c), and Cu (Figure 4e), demonstrating that three different metals can be deposited into a single template. Additionally, for Au, we also deposited metal into the gyroid minority PPC pores of the Q^{230} core−shell double gyroid structure of PI-*b*-PS-*b*-PPC-3 (Figure 4b), demonstrating that orthogonal degradation can be used to fabricate metal networks with different structures. We backfilled Ni metal into the PPC minority network of the O^{70} template (PI-*b*-PS-*b*-PPC-1, Figure 4d) and backfilled Cu metal into the PI minority network pores from the Q^{214} template (PI-*b*-PS-*b*-PPC-2, Figure 4f), verifying metal backfilling is not specific to only the Q^{230} core−shell double gyroid structure. Deposition of Au metal into the polymer templates resulted in patchy coverage of areas 100−1000 nm in size, depending on distance of the Au gyroid from the film surface. Patchy deposition of Au metal could be the result of the use of sodium borohydride rather than hydrazine[47] as a reducing agent or the result of decomposition of the plating solution. We expect future optimization of the Au plating solutions would result in more uniform deposition of Au metal throughout the mesoporous template. Alternatively, Ni and Cu metal both resulted in more uniform metal deposition throughout the film. With this work, we demonstrated that three different metals could be deposited into the PI and PPC pores of the various networked templates. SEM micrographs of freestanding Au and Ni networks after removal of the remaining organic material are available in Supporting Figures S14−S16.

Orthogonal Deposition of Two Metals into PI-*b*-PS-*b*-PPC Triblock Terpolymer Templates. As a proof of principle, we demonstrated first steps of the orthogonal deposition of Au and Cu metal networks into a single polymer template using sequential degradation and backfilling of the resulting mesopores. Although seeded growth deposition of Au metal was the least uniform throughout the templates, we used Au deposition due to the chemical resistance of Au metal to acidic and basic conditions as well as other metal precursor solutions.

After degradation of the PI block, Au metal was deposited into the mesoporous templates of PI-*b*-PS-*b*-PPC-4. Following Au deposition, the PPC block was degraded using a NaOH solution. No adverse effects on the Au gyroids were observed. Cu metal was subsequently deposited orthogonally into the PPC pores. The PS block was left behind in the template and was unaffected by the degradation or backfilling process. The deposition of both metals was first characterized by TEM (Figure 5a). Because of the incomplete backfilling of the PI pores with Au, we expected that electroless deposition would deposit Cu metal not only into the PPC pores of the structure but rather into any remaining void space not occupied by Au,

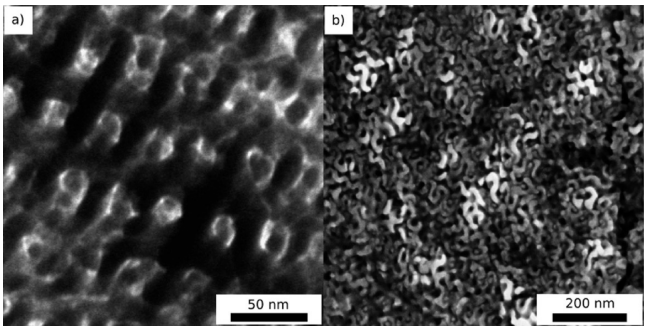

Figure 5. Orthogonal deposition of Au and Cu metal into PI-*b*-PS-*b*-PPC-4 triblock terpolymer templates. (a) TEM micrograph of Au and Cu metal networks; dark regions indicate the presence of metal. (b) SEM micrograph (secondary electron detector) of Au and Cu metal networks; PS block was removed using dissolution in THF.

DOI: 10.1021/jacs.5b01915
J. Am. Chem. Soc. 2015, 137, 6026−6033

including the remaining matrix PI pores. This is exactly what was observed in the imaging experiments. Although the micrograph from Figure 5a is consistent with deposition of metal into both the matrix and gyroid minority networks of the structure, such micrographs alone were insufficient to elucidate exactly where each metal was located within the structure. As a first effort along these lines, the PS block was removed using dissolution in THF to leave behind freestanding Au and Cu metal networks, which were then imaged using SEM (Figure 5b). While SEM micrographs were consistent with both sets of pores being filled, they also did not further elucidate exact metal locations.

Therefore, we turned our attention to high-angle annular dark field scanning transmission electron microscopy (HAADF STEM) to distinguish the Au and Cu networks due to increased contrast between the two metals. In HAADF STEM imaging, contrast between two materials is proportional to roughly the square of the atomic number, $Z^{1.7}$. HAADF STEM micrographs of two different projections of the same hybrid imaged in Figure 5 are shown in Figure 6a,b. The STEM

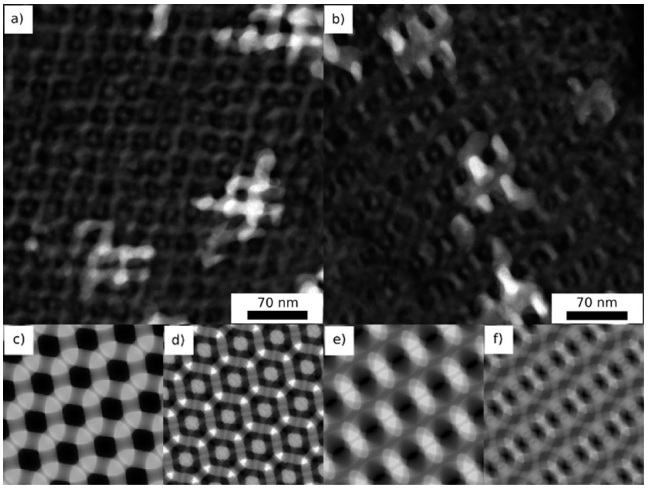

Figure 6. HAADF STEM micrographs of Au and Cu metal networks from PI-*b*-PS-*b*-PPC-4 terpolymer templates. (a,b) HAADF STEM micrographs of Au and Cu networks in single template; bright regions indicate Au metal, while gray regions indicate Cu metal. Black regions indicate vacuum or organic material. (c–f) Incoherent STEM simulations of Q^{230} double gyroid metal structures. Metal networks appear bright while organic domains remain dark. (c,e) Simulations of projections in (a,b) with Au metal only in the matrix (majority) network pores. (d,f) Simulations of projections in (a,b) with Cu metal in both majority network and minority network pores.

micrograph in Figure 6a is consistent with the [110] projection of the Q^{230} core–shell double gyroid. Likewise, the STEM micrograph in Figure 6b is consistent with the [210] projection of the Q^{230} double gyroid structure. Bright regions correspond to higher atomic number Au networks, while lighter gray regions correspond to Cu gyroid networks. Figure 6 clearly demonstrates that orthogonally degrading and backfilling the different pore spaces with two different inorganic (metal) compounds was successful. This is corroborated by basic STEM projection simulations of the [110] and [210] projections with Au metal in double-gyroid majority network (matrix PI derived) pores only (Figure 6c,e) and Cu metal in both gyroid majority and minority network (PI and PPC derived) pores (Figure 6d,f), which are consistent with the experimental STEM micrographs in Figure 6a,b. One detail that became evident from analyzing these images is that the gold strut size appears bigger than that of the Cu deposits. This may be attributed to distortions of the block copolymer template structure during or after deposition of Au. The fact that we saw this only for Au and not for Cu is consistent with higher surface mobility of Au at moderate temperatures, particularly in nanostructures.[49] The STEM projection simulations in Figure 6c–f were generated to reflect the differences in strut size between Au and Cu metals. Finally, in order to further elucidate the three-dimensional (3D) character of both networked metal deposits, we reconstructed a 3D model of the sample using HAADF STEM tomography (Figure 7a and 7b). The

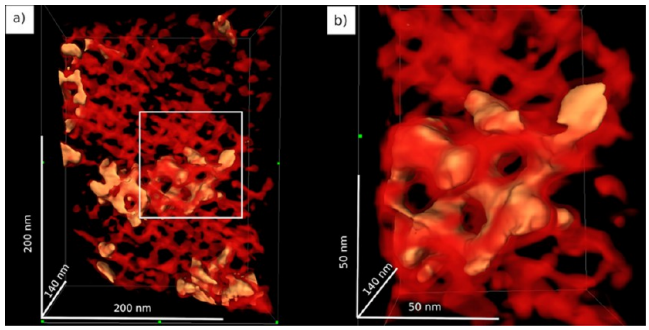

Figure 7. 3D reconstruction of Au and Cu metal networks from PI-*b*-PS-*b*-PPC-4 terpolymer templates. (a,b) 3D reconstruction with HAADF STEM tomography of Au (yellow isosurface rendering) and Cu (red volume rendering) metal networks where red regions indicate Cu metal and yellow regions indicate Au metal. (a) Large-area reconstructed region and (b) close up of region contained in white box in (a) revealing both Cu and Au networks.

reconstruction clearly shows that both metals, Au (yellow) and Cu (red) are network structures. A movie created from the HAADF STEM tilt series is available in the Supporting Information.

CONCLUSIONS

In summary, we report the synthesis of a new orthogonally degradable PI-*b*-PS-*b*-PPC triblock terpolymer and the deposition of multiple metals into the resulting porous structures using sequential degradation and backfilling. We synthesized the PI-*b*-PS-*b*-PPC triblock terpolymers using a combination of anionic and rapid chain-shuttling polymerization and identified regions in the phase space where the triblock terpolymers self-assembled into cocontinuous network morphologies. We orthogonally degraded the PI and PPC blocks of various networked terpolymers to yield ordered mesoporous templates. We deposited Au, Ni, and Cu metal separately into porous networks produced from degradation of the PI and PPC blocks. Finally, we sequentially degraded the PI and PPC blocks and backfilled the structure with Au and Cu metal to show proof-of-principle for the fabrication of three-component polymer–inorganic hybrid materials where the Au and Cu metals form separate continuous networks. Removal of the final PS blocks resulted in networked binary metal structures. We anticipate the deposition of multiple materials can be expanded to include different combinations of metals, metal oxides, and ceramic materials for a variety of applications including tandem and size-selective catalysis.

DOI: 10.1021/jacs.5b01915
J. Am. Chem. Soc. 2015, 137, 6026–6033

■ ASSOCIATED CONTENT

Supporting Information

Synthetic details; electron microscopy protocols; ^{1}H NMR spectra; polymer characterization; SAXS patterns; TEM micrographs; additional SEM micrographs; movie created from STEM tilt series. This material is available free of charge via the Internet at http://pubs.acs.org.

■ AUTHOR INFORMATION

Corresponding Authors

*coates@cornell.edu

*ubw1@cornell.edu

Present Address

$^{\perp}$3M Company, Saint Paul, Minnesota 55144, United States.

Notes

The authors declare no competing financial interest.

■ ACKNOWLEDGMENTS

We thank the National Science Foundation for support (DMR-1409105 and CHE-1112278). Electron microscopy characterization was supported by the Energy Materials Center at Cornell (EMC^2), an Energy Frontier Research Center funded by the U.S. Department of Energy, Office of Science, Office of Basic Energy Sciences under Award Number DE-SC0001086. C.D.C. is the recipient of an NSF Graduate Research Fellowship Program (GRFP) fellowship (DGE-1144153) and acknowledges support from the NSF IGERT program (DGE-0654193). This work was produced using Cornell Center for Materials Research (CCMR) facilities (DMR-1120296). Characterization was done in part at Cornell High Energy Synchrotron Source (CHESS) funded by the National Science Foundation and the National Institutes of Health/National Institute of General Medical Sciences under NSF award DMR-0936384. Facilities were provided in part by the King Abdullah University of Science and Technology (KAUST)-Cornell Center for Energy and Sustainability. The authors gratefully acknowledge Mr. Joerg Werner and Mr. Peter Beaucage for assistance with SAXS measurements.

■ REFERENCES

(1) Meuler, A. J.; Hillmyer, M. A.; Bates, F. S. *Macromolecules* **2009**, *42*, 7221−7250.

(2) Bates, F. S.; Fredrickson, G. H. *Phys. Today* **1999**, *52*, 32−38.

(3) Templin, M.; Du Chesne, A.; Franck, A.; Leist, H.; Zhang, Y.; Ulrich, R.; Shadler, V.; Wiesner, U. *Science* **1997**, *278*, 1795−1798.

(4) Yang, P.; Deng, T.; Zhao, D.; Feng, P.; Pine, D.; Chmelka, B. F.; Whitesides, G. M.; Stucky, G. D. *Science* **1998**, *282*, 2244−2246.

(5) Gier, T. E.; Bu, X.; Feng, P.; Stucky, G. D. *Nature* **1998**, *395*, 154−157.

(6) Joo, S. H.; Choi, S. J.; Oh, I.; Kwak, J.; Liu, Z.; Terasaki, O.; Ryoo, R. *Nature* **2001**, *412*, 169−172.

(7) Warren, S. C.; Messina, L. C.; Slaughter, L. S.; Kamperman, M.; Zhou, Q.; Gruner, S. M.; DiSalvo, F. J.; Wiesner, U. *Science* **2008**, *320*, 1748−1752.

(8) Arora, H.; Du, P.; Tan, K. W.; Hyun, J. K.; Grazul, J.; Xin, H. L.; Muller, D. A.; Thompson, M. O.; Wiesner, U. *Science* **2010**, *330*, 214−219.

(9) Hillmyer, M. A. *Adv. Polym. Sci.* **2005**, *190*, 137−181.

(10) Vukovic, I.; ten Brinke, G.; Loos, K. *Polymer* **2013**, *54*, 2591−2605.

(11) Hashimoto, T.; Tsutsumi, K.; Funaki, Y. *Langmuir* **1997**, *13*, 6869−6872.

(12) Thurn-Albrecht, T.; Schotter, J.; Kaestle, G. A.; Emley, N.; Shibauchi, T.; Krusin-Elbaum, L.; Guarini, K.; Black, C. T.; Tuominen, M.; Russell, T. P. *Science* **2000**, *290*, 2126−2129.

(13) Vignolini, S.; Yufa, N. A.; Cunha, P. S.; Guldin, S.; Rushkin, I.; Stefik, M.; Hur, K.; Wiesner, U.; Baumberg, J. J.; Steiner, U. *Adv. Mater.* **2012**, *24*, OP23−OP27.

(14) Crossland, E. J. W.; Kamperman, M.; Nedelcu, M.; Ducati, C.; Wiesner, U.; Smilgies, D.-M.; Toombes, G. E. S.; Hillmyer, M. A.; Ludwigs, S.; Steiner, U.; Snaith, H. J. *Nano Lett.* **2009**, *9*, 2807−2812.

(15) Scherer, M. R. J.; Cunha, P. M. S.; Steiner, U. *Adv. Mater.* **2014**, *26*, 2403−2407.

(16) Bockstaller, M. R.; Lapetnikov, Y.; Margel, S.; Thomas, E. L. *J. Am. Chem. Soc.* **2003**, *125*, 5276−5277.

(17) Li, Z.; Hur, K.; Sai, H.; Higuchi, T.; Takahara, A.; Jinnai, H.; Gruner, S. M.; Wiesner, U. *Nat. Commun.* **2014**, *5*, 3247.

(18) Horechyy, A.; Nandan, B.; Zafeiropoulos, N. E.; Formanek, P.; Oertel, U.; Bigall, N. C.; Eychmüller, A.; Stamm, M. *Adv. Funct. Mater.* **2013**, *23*, 483−490.

(19) Tyler, C. A.; Qin, J.; Bates, F. S.; Morse, D. C. *Macromolecules* **2007**, *40*, 4654−4668.

(20) Stefik, M.; Wang, S.; Hovden, R.; Sai, H.; Tate, M. W.; Muller, D. A.; Steiner, U.; Gruner, S. M.; Wiesner, U. *J. Mater. Chem.* **2012**, *22*, 1078−1087.

(21) Cohen, C. T.; Chu, T.; Coates, G. W. *J. Am. Chem. Soc.* **2005**, *127*, 10869−10878.

(22) Inoue, S. *J. Polym. Sci., Part A: Polym. Chem.* **2000**, *38*, 2861−2871.

(23) Asano, S.; Aida, T.; Inoue, S. *J. Chem. Soc., Chem. Commun.* **1985**, 1148−1149.

(24) Bailey, T. S.; Pham, H. D.; Bates, F. S. *Macromolecules* **2001**, *34*, 6994−7008.

(25) Allen, S. D.; Coates, G. W.; Cherian, A. E.; Simoneau, C. A.; Gridnev, A. A.; Farmer, J. J. U.S. Patent. 8,247,520, 2009.

(26) Lu, X.-B.; Darensbourg, D. J. *Chem. Soc. Rev.* **2012**, *41*, 1462−1484.

(27) Wang, Y.-M.; Song, X.-Y.; Shao, S.-H.; Xu, P.-X.; Ren, W.-M.; Lu, X.-B. *Polym. Chem.* **2013**, *4*, 629−636.

(28) Epps, T. H.; Cochran, E. W.; Bailey, T. S.; Waletzko, R. S.; Hardy, C. M.; Bates, F. S. *Macromolecules* **2004**, *37*, 8325−8341.

(29) Epps, T. H.; Cochran, E. W.; Hardy, C. M.; Bailey, T. S.; Waletzko, R. S.; Bates, F. S. *Macromolecules* **2004**, *37*, 7085−7088.

(30) Bailey, T. S.; Hardy, C. M.; Epps, T. H. I.; Bates, F. S. *Macromolecules* **2002**, *35*, 7007−7017.

(31) Chatterjee, J.; Jain, S.; Bates, F. S. *Macromolecules* **2007**, *40*, 2882−2896.

(32) Salvatore, S.; Demetriadou, A.; Vignolini, S.; Oh, S. S.; Wuestner, S.; Yufa, N. A.; Stefik, M.; Wiesner, U.; Baumberg, J. J.; Hess, O.; Steiner, U. *Adv. Mater.* **2013**, *25*, 2713−2716.

(33) Park, M.; Harrison, C.; Chaikin, P. M.; Register, R. A.; Adamson, D. H. *Science* **1997**, *276*, 1401−1404.

(34) Zalusky, A. S.; Olayo-Valles, R.; Wolf, J. H.; Hillmyer, M. A. *J. Am. Chem. Soc.* **2002**, *124*, 12761−12773.

(35) Thurn-Albrecht, T.; Steiner, R.; Derouchey, J.; Stafford, C. M.; Huang, E.; Bal, M.; Tuominen, M.; Hawker, C. J.; Russell, T. P. *Adv. Mater.* **2000**, *12*, 787−791.

(36) Mao, H.; Hillmyer, M. A. *Macromolecules* **2005**, *38*, 4038−4039.

(37) Sedransk, K. L.; Kaminski, C. F.; Hutchings, L. R.; Moggridge, G. D. *Polym. Degrad. Stab.* **2011**, *96*, 1074−1080.

(38) Bertrand, A.; Hillmyer, M. A. *J. Am. Chem. Soc.* **2013**, *135*, 10918−10921.

(39) Chang, C.; Emrick, T. *Macromolecules* **2014**, *47*, 1344−1350.

(40) Guo, S.; Rzayev, J.; Bailey, T. S.; Zalusky, A. S.; Olayo-Valles, R.; Hillmyer, M. A. *Chem. Mater.* **2006**, *18*, 1719−1721.

(41) Tang, C.; Sivanandan, K.; Stahl, B. C.; Fredrickson, G. H.; Kramer, E. J.; Hawker, C. J. *ACS Nano* **2010**, *4*, 285−291.

(42) Hsueh, H.-Y.; Huang, Y.-C.; Ho, R.-M.; Lai, C.-H.; Makida, T.; Hasegawa, H. *Adv. Mater.* **2011**, *23*, 3041−3046.

DOI: 10.1021/jacs.5b01915
J. Am. Chem. Soc. 2015, 137, 6026−6033

(43) Du Sart, G. G.; Vukovic, I.; Vukovic, Z.; Polushkin, E.; Hiekkataipale, P.; Ruokolainen, J.; Loos, K.; ten Brinke, G. *Macromol. Rapid Commun.* **2011**, *32*, 366−370.
(44) Tappan, B. C.; Steiner, S. A.; Luther, E. P. *Angew. Chem., Int. Ed.* **2010**, *49*, 4544−4565.
(45) dos Santos, K. A. M.; Suarez, P. A. Z.; Rubim, J. C. *Polym. Degrad. Stab.* **2005**, *90*, 34−43.
(46) Blach, J. A.; Watson, G. S.; Busfield, W. K.; Myhra, S. *Polym. Int.* **2002**, *51*, 12−20.
(47) Hsueh, H.-Y.; Chen, H.-Y.; Hung, Y.-C.; Ling, Y.-C.; Gwo, S.; Ho, R.-M. *Adv. Mater.* **2013**, *25*, 1780−1786.
(48) Zehner, R. W.; Sita, L. R. *Langmuir* **1999**, *15*, 6139−6141.
(49) Biener, J.; Wittstock, A.; Biener, M. M.; Nowitzki, T.; Hamza, A. V.; Baeumer, M. *Langmuir* **2010**, *26*, 13736−13740.

DOI: 10.1021/jacs.5b01915
J. Am. Chem. Soc. 2015, 137, 6026−6033